On the Privacy Risks of Cell-Based NAS Architectures

Hai Huang
CISPA Helmholtz Center for Information Security

Zhikun Zhang
CISPA Helmholtz Center for Information Security

Yun Shen
NetApp

Michael Backes
CISPA Helmholtz Center for Information Security

Qi Li
Tsinghua University & Zhongguancun Lab

Yang Zhang
CISPA Helmholtz Center for Information Security

ABSTRACT

Existing studies on neural architecture search (NAS) mainly focus on efficiently and effectively searching for network architectures with better performance. Little progress has been made to systematically understand if the NAS-searched architectures are robust to privacy attacks while abundant work has already shown that human-designed architectures are prone to privacy attacks. In this paper, we fill this gap and systematically measure the privacy risks of NAS architectures. Leveraging the insights from our measurement study, we further explore the cell patterns of cell-based NAS architectures and evaluate how the cell patterns affect the privacy risks of NAS-searched architectures. Through extensive experiments, we shed light on how to design robust NAS architectures against privacy attacks, and also offer a general methodology to understand the hidden correlation between the NAS-searched architectures and other privacy risks.[1]

CCS CONCEPTS

• **Security and privacy**; • **Computing methodologies** → **Machine learning**;

KEYWORDS

neural architecture search; membership inference attacks; cell patterns

ACM Reference Format:
Hai Huang, Zhikun Zhang, Yun Shen, Michael Backes, Qi Li, and Yang Zhang. 2022. On the Privacy Risks of Cell-Based NAS Architectures. In *Proceedings of the 2022 ACM SIGSAC Conference on Computer and Communications Security (CCS '22), November 7–11, 2022, Los Angeles, CA, USA.* ACM, New York, NY, USA, 15 pages. https://doi.org/10.1145/3548606.3560619

1 INTRODUCTION

Deep neural networks (DNNs) have enjoyed a remarkable boom in recent decades and achieved superior performance in many real-world tasks (e.g., image classification [28, 38, 67], object detection [46, 60], text classification [36, 79], etc.). With significant advances in computing power, DNNs have become more complicated. They are both deeper [49, 61] and wider [49, 50] to further improve model performance (e.g., GPT-1/2/3 [4, 56, 57], DALL-E [59], etc.). Despite their success, manually designing those complex networks in a trial-and-error way remains a tedious task, requiring both architectural engineering skills and domain expertise.

Neural architecture search (NAS) [3, 86] is a natural step towards resolving the above challenge. It aims at automating the search process for the most suitable deep neural network architectures for specific tasks. The core idea of NAS is using a *search strategy* to select an architecture from a predefined *search space*, and leverage a performance estimation strategy to guide the search process. Directly searching all eligible architectures is computationally expensive; thus the mainstream cell-based NAS methods treat the whole network architecture as a combination of specific modules to reduce the search space (Figure 1 illustrates a typical cell-based NAS architecture). Previous work has shown that the architectures selected by cell-based NAS techniques can attain comparable performance or even outperform those traditional human-designed architectures on tasks such as image classification [23, 39, 87], object detection [22, 72], etc. Existing NAS research mainly focuses on two directions — identify efficient and effective search strategies to obtain the best architecture candidates [2, 10, 73] and improve the robustness of NAS-searched architectures against adversarial examples [15, 24, 41]. On the other hand, although abundant work has already shown that human-designed architectures are prone to privacy attacks, little progress has been made to systematically understand if the NAS-searched architectures are robust to privacy attacks given their complex network topology [54]. In privacy attacks, an adversary's goal is to gain knowledge of the target model's training data, which is not intended to be shared. The most popular attack in this domain is membership inference attack (MIA) [64] which enables an attacker to infer whether a sample is used to train a target model. So far, little attention has been paid on the membership privacy of NAS-searched architectures.

Our Work. In this paper, we focus on the aforementioned membership inference attack against NAS-searched architectures due to its pervasiveness and the privacy impact in the real world. Concretely, we address two research questions in this study — *whether NAS-searched architectures are robust to membership inference attacks* and *how architectural information affects such robustness.* Note that the first research question has been discussed by some preliminary work [54] in a limited scenario, i.e., label-only membership inference [13, 43].

[1]The source code of our experiments can be found at https://github.com/MiracleHH/nas_privacy

CCS '22, November 7–11, 2022, Los Angeles, CA, USA

ACM ISBN 978-1-4503-9450-5/22/11…$15.00
https://doi.org/10.1145/3548606.3560619

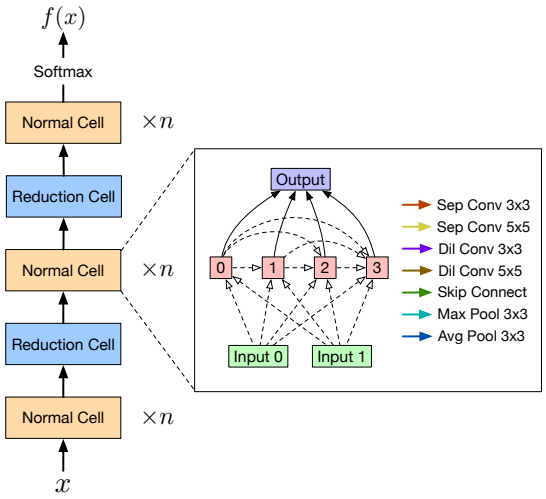

Figure 1: Illustration of the cell-based NAS architecture. The normal and reduction cells are repeated multiple times and connected together to constitute the whole network architecture, and the cell structures for normal and reduction cells will be searched in the search process of NAS. In the box on the right, there is a general DARTS [44] search space prototype where the arrows with dashed lines represent possible edges and each selected edge will be assigned with one operation indicated by one colored arrow on the right.

To this end, we first conduct a comprehensive measurement study to systematically evaluate the privacy risks of NAS-searched architectures identified by cell-based NAS algorithms, the most popular and influential NAS methods [70]. We find that NAS-searched architectures are generally more robust against MIAs. For instance, 9 out of 10 NAS-searched architectures are more robust to membership inference attacks than all other 10 human-designed architectures for the ⟨Black-Box, Shadow⟩ attack setting (see Section 3 for more details) on the CIFAR10 dataset [1] in our study. Interestingly, our findings show that the robustness against MIAs varies from architecture to architecture. As we see in Figure 3, it is evident that certain NAS-searched architectures are more vulnerable to MIAs than others. For example, architectures searched by TENAS [10] tend to be more prone to membership inference attacks.

Following the new insights from our measurement study, we move on to understand how different internal structures impact the privacy robustness of NAS-searched architectures. To this end, we introduce a general framework to extract cell patterns related to MIA performance (see Section 4). Concretely, we first evaluate the MIA effectiveness on the well-performed architectures, and then extract the cell patterns for the relatively vulnerable and robust architectures separately under the assistance of a regression model. Here, this regression model is trained with the former evaluation results to give direct MIA performance predictions on cell architectures. Finally, we use the extracted cell patterns to modify the internal structures of the target cell architectures and compare the MIA performance before and after the modifications to estimate the effectiveness of the cell patterns. This framework is generic and can be applied to any other analysis work similar to our objective. Following this framework, we evaluate the MIA performance of 2,678 NAS-searched architectures from the NAS-Bench-301 dataset [66] and show that we can identify certain cell patterns that promote or demote MIA performance.

We further apply our analysis framework to mitigating MIA on NAS-searched architectures. The evaluation results show that our cell patterns can successfully promote or demote the MIA performance on the target NAS architectures in the majority of cases. In addition, our cell patterns, though extracted from NAS-Bench-301 dataset, can be transferred to different datasets, attacks, and search spaces. Finally, we show that our work is complementary to existing MIA defense mechanisms when applying the MIA demotion cell patterns to the target NAS architectures, and can further enhance the effectiveness of existing defense strategies. We hope that our findings will inspire future work on designing more robust NAS architectures against membership leakage.

Contributions. In summary, we make the following contributions.

- We systematically evaluate the privacy risks of NAS-searched architectures. Through extensive experiments on four datasets, we show that NAS-searched architectures are usually more robust than human-designed architectures. Our finding is contrary to the results from Pang et al. [54]. However, the privacy risks of the NAS-searched architectures must be individually evaluated.
- We introduce a general framework to analyze the relationship between the NAS-searched architectures and corresponding privacy attacks. We successfully instantiate it to understand, analyze, and identify the hidden cell patterns that impact MIA performance.
- We explore the correlation between the NAS-searched architectures and the robustness against MIAs and identify certain cell patterns that impact MIA performance. The experimental results show that our cell patterns can successfully demote or promote MIA performance on target NAS architectures in most cases. Furthermore, our cell patterns can transfer to new attack settings and are complementary to existing defense work.

2 PRELIMINARIES

2.1 Cell-based Neural Architecture Search

Overview. The *search space* of NAS can be extremely large if we directly search for and enumerate every single candidate structure of the whole network. To cope with this challenge, *cell-based* NAS algorithms treat the whole network architecture as a combination of specific small modules, which is referred to as *cells*. As such, we only need to search for the structures of the basic cells, which significantly reduces the search space and speeds up the search process. Due to the outstanding performance and high flexibility, cell-based NAS algorithms have dominated the NAS research [70]. Figure 1 illustrates a typical cell-based NAS architecture.

There are usually two types of cells in such architectures, *normal cell* and *reduction cell*. The normal cell preserves the dimension of the input, while the reduction cell reduces the spatial dimension of the input. The reduction cells are usually placed at the 1/3 and 2/3 positions of the total number of cells, and the rest are normal cells [44]. Under this setting, a cell-based NAS architecture usually has only two reduction cells and tends to have more normal cells especially when the network is deep. Both normal and reduction cells

are composed of topological combinations of candidate operations (e.g., separable convolution and skip connection).

The discrete candidate operations can be represented as continuous architectural parameters such that the whole architecture can be differentially optimized regarding both the model weights and architectural parameters in the search process. We can gradually train a super network that contains all possible edges in a cell to search for suitable structures of both normal and reduction cells. When we evaluate the performance of candidate architectures, only a limited number (e.g., 2) of input edges with the highest architectural parameters for each intermediate node in the cell will be retained as real corresponding operations. The model weights will be inherited from the super network by the current candidate architecture to evaluate the performance on a validation dataset. In this way, the search space and computation cost are significantly reduced compared to previous NAS methods.

DARTS. We use DARTS [44], the most typical cell-based NAS algorithm, to demonstrate the general concepts and workflow of the cell-based NAS methods. The right box of Figure 1 illustrates the cell search space of the DARTS algorithm, which is represented by a directed acyclic graph (DAG) containing 7 nodes, i.e., 2 input nodes, 4 intermediate nodes, and 1 output node, and multiple edges. The nodes represent the state of the data, and the edges represent the operations on the data. The operation $o^{(i,j)}$ between node i and j is selected from a predefined *operation set* containing $K = 7$ different operations. For an intermediate node j, it obtains the intermediate data $x^{(j)}$ by aggregating all of its predecessors, i.e., $x^{(j)} = \sum_{i<j} o^{(i,j)} x^{(i)}$. The outputs of all intermediate nodes will be concatenated to the output node in the end. In the final cell architecture, each intermediate node is only allowed to have 2 input nodes. Therefore, though there are 14 possible edges to connect intermediate nodes in Figure 1, we can only choose ($4 \times 2 = 8$) edges from them and fill these edges with the most likely operations. For simplicity, we refer to the search space defined in the DARTS algorithm as *DARTS search space*. Note that, there are also some other kinds of search spaces, the most representative one among them is NAS-Bench-201 [18], a much simpler and smaller search space. More details can be found in Appendix C of our technical report [31]. [2]

2.2 Membership Inference Attack

Membership inference attacks (MIAs) against machine learning models aim to infer whether a target sample x is used to train a target model f_{target}. As such, MIA directly leads to a privacy breach, allowing the adversaries to learn sensitive information about the training data. For example, in the real world, x can be a clinical record or an individual. MIA enables the attackers can infer whether this clinical record or individual has been used to train a model associated with a certain disease. This is evidently a privacy and confidentiality violation.

Consider the most common attack setting where the adversary has black-box access to the target model [64], to launch such an attack, the attackers first train a shadow model f_{shadow} using a shadow dataset $\mathcal{D}^{\text{train}}_{\text{shadow}}$, which performs the same task as f_{target} (e.g., classification). The attackers then query f_{shadow} using both $\mathcal{D}^{\text{train}}_{\text{shadow}}$ (member data) and $\mathcal{D}^{\text{test}}_{\text{shadow}}$ (non-member data) and obtain the query responses $R = R_{\text{member}} \cup R_{\text{non-member}}$. They can build an attack model $f_{\text{attack}} : R \rightarrow \{0, 1\}$, where the responses of member data are labeled as 1 and those of non-member are labeled as 0. At the attack time, the attackers query f_{target} using the data instance x and use f_{attack} to infer whether $x \in \mathcal{D}^{\text{train}}_{\text{target}}$ or not using the response from the target model f_{target}.

[2] Due to space limitation, we defer all the appendices to our technical report [31]

3 PRIVACY MEASUREMENT OF NAS-SEARCHED ARCHITECTURES

3.1 Motivation

Many papers point out that overfitting of the target ML models (i.e., the target model performs much better on its training data than test data) is the main factor contributing to the success of MIAs [47, 62, 64, 80]. Shu et al. [65] show that the cell architectures searched by cell-based NAS tend to be shallow and wide to make the loss value converge stably and fast during the search process, which usually leads to competitive generalization performance though it is not guaranteed to be the best. In other words, the architectures searched by these NAS algorithms usually have low overfitting levels. Therefore, a natural hypothesis is that NAS-searched architectures are more robust against MIAs than traditional human-designed ones. Yet, recent work from Pang et al. [54], using empirical results, demonstrates that the NAS architectures are more vulnerable to MIAs than those human-designed architectures, even though the former have better normal model performance than the latter. Note that the conclusion of Pang et al. [54] is based on the label-only scenario for MIA in a black-box setting. In light of the conflicting results, in this section, we comprehensively evaluate the performance of MIAs on NAS-searched architectures and human-designed architectures in both black-box and white-box settings with different levels of knowledge. Our goal is to eliminate the potential experimental bias introduced in the previous research and compare the MIA performance on both categories in a wider spectrum of attack scenarios.

3.2 Measurement Setting

Datasets. We use 4 diverse benchmark datasets to conduct the measurement experiments, including CIFAR10 [1], CIFAR100 [1], STL10 [14], and CelebA [48]. We refer the readers to Appendix A of our technical report [31] for the details of these datasets.

NAS Algorithms. We use 10 representative NAS algorithms to conduct the experiments: (1) DARTS-V1 [44]; (2) DARTS-V2 [44]; (3) ENAS [55]; (4) GDAS [17]; (5) SETN [16]; (6) Random [5]; (7) TENAS [10]; (8) DrNAS [12]; (9) PC-DARTS [78]; (10) SDARTS [11]. We defer the detailed description of them to Appendix A of our technical report [31].

Manual Architectures. For comparison, we also select 10 representative human-designed architectures to conduct the experiments: (1) ResNet [25]; (2) ResNext [76]; (3) WideResNet [82]; (4) VGG [67]; (5) DenseNet [30]; (6) EfficientNet [69]; (7) RegNet [58]; (8) CSPNet [71]; (9) BiT [37]; (10) DLA [81]. We refer the readers to Appendix A of our technical report [31] for the details of these architectures.

Data Configuration. To facilitate the fair comparison of different MIA methods, we split the original dataset $\mathcal{D}$ into 4 disjoint parts with the same size, i.e., $\mathcal{D}^{\text{train}}_{\text{target}}$, $\mathcal{D}^{\text{test}}_{\text{target}}$, $\mathcal{D}^{\text{train}}_{\text{shadow}}$ and $\mathcal{D}^{\text{test}}_{\text{shadow}}$. $\mathcal{D}^{\text{train}}_{\text{target}}$ and $\mathcal{D}^{\text{test}}_{\text{target}}$ serve as the training and testing dataset of the target model, while $\mathcal{D}^{\text{train}}_{\text{shadow}}$ and $\mathcal{D}^{\text{test}}_{\text{shadow}}$ are utilized as the training and testing dataset of the shadow model. As for the NAS algorithm, we further split $\mathcal{D}^{\text{train}}_{\text{target}}$ into two disjoint parts with the same size to obtain $\mathcal{D}^{\text{train}^{\text{t}}}_{\text{target}}$ and $\mathcal{D}^{\text{train}^{\text{v}}}_{\text{target}}$, where $\mathcal{D}^{\text{train}^{\text{t}}}_{\text{target}}$ and $\mathcal{D}^{\text{train}^{\text{v}}}_{\text{target}}$ are used as the training and validation datasets respectively of the NAS algorithm in the search process. After the final NAS architecture is generated, we train it from scratch using $\mathcal{D}^{\text{train}}_{\text{target}}$ and test its performance on $\mathcal{D}^{\text{test}}_{\text{target}}$. Note that our NAS training/validation data split is in line with the latest research by Oymak et al. [53], which states that the train-validation accuracy gap decreases rapidly when the validation data is mildly large. Take CIFAR10 dataset for example, the size of $\mathcal{D}^{\text{train}^{\text{v}}}_{\text{target}}$ is 7,500, which is fairly sizeable and matching the recommendation by Oymak et al. [53]. In turn, we are more likely to make our NAS-searched architectures achieve better generalization performance.

Attacker's Knowledge. According to the different knowledge levels the attacker has about the target model, we classify the existing MIAs into 5 types and use them to evaluate the above 10 NAS algorithms and 10 human-designed models. In this way, we can conduct a thorough and objective evaluation of both NAS-searched and human-designed architectures in all known MIA attach scenarios [29, 47].

- ⟨Black-Box, Shadow⟩. In this scenario, the attacker only has black-box access to the target model with a local shadow dataset and does not know the training dataset of the target model.
- ⟨Black-Box, Partial⟩. The attacker has black-box access to the target model and has partial knowledge of the training dataset of the target model.
- ⟨White-Box, Shadow⟩. The attacker has white-box access to the target model with only a local shadow dataset and does not know the training dataset of the target model.
- ⟨White-Box, Partial⟩. The attacker has white-box access to the target model and has partial knowledge of the training dataset of the target model. This is the strongest attack scenario.
- ⟨Label-Only⟩. The attacker only has black-box access to the target model and can only infer information from the output labels of the target model, which is the weakest attack scenario.

Note that the attacker obtains all confidence scores returned by the target model except for the ⟨Label-Only⟩ MIA scenario. We defer the training details of the target models and attack models to Appendix A of our technical report [31].

3.3 Measurement Results

Model Performance. The model performance and overfitting of both NAS-search and human-designed models on 4 benchmark datasets are shown in Table 1. We can observe that the performance of the architectures searched by NAS is comparable to or even better than that of the human-designed architectures. Our model performance results are consistent with the previous research from both the ML community [11, 87] and Pang et al. [54]. The overfitting levels on the CIFAR100 and STL10 datasets are relatively high due to the fact that the test accuracy on these two datasets is much lower than that on the CIFAR10 and CelebA datasets, and the training accuracy on all four datasets can reach round 1.0 for most architectures under the same training settings. We can see that, most architectures comply with the general rule that a higher test accuracy tends to lead to a lower overfitting level.

Table 1: Normal test accuracy of NAS-searched and human-designed architectures on four different datasets. The numbers in the parentheses stand for the corresponding overfitting levels.

	Architecture	Dataset			
		CIFAR10	CIFAR100	STL10	CelebA
Human-designed	ResNet	0.6587 (0.3413)	0.2993 (0.7005)	0.4948 (0.5052)	0.7438 (0.2562)
	ResNext	0.6410 (0.3590)	0.3026 (0.6973)	0.4711 (0.5289)	0.7468 (0.2532)
	WideResNet	0.6431 (0.3569)	0.3028 (0.6971)	0.4662 (0.5338)	0.7516 (0.2484)
	VGG	0.7796 (0.2204)	0.4395 (0.5603)	0.6102 (0.3895)	0.7627 (0.2373)
	DenseNet	0.7509 (0.2491)	0.4128 (0.5871)	0.5815 (0.4185)	0.7506 (0.2494)
	EfficientNet	0.5637 (0.4360)	0.2401 (0.7597)	0.3862 (0.6132)	0.7240 (0.2687)
	RegNet	0.5360 (0.4640)	0.2252 (0.7744)	0.4206 (0.5794)	0.7366 (0.2632)
	CSPNet	0.6745 (0.3255)	0.3151 (0.6848)	0.5169 (0.4831)	0.7434 (0.2566)
	BiT	0.6165 (0.3835)	0.2417 (0.7581)	0.4274 (0.5726)	0.7401 (0.2599)
	DLA	0.6245 (0.3755)	0.3049 (0.6948)	0.4517 (0.5483)	0.7411 (0.2589)
NAS-searched	DARTS-V1	0.7043 (0.0979)	0.4071 (0.5929)	0.5917 (0.0911)	0.7663 (0.0272)
	DARTS-V2	0.7028 (0.0962)	0.3895 (0.6105)	0.6123 (0.3877)	0.7704 (0.0777)
	ENAS	0.6343 (0.0270)	0.3895 (0.6057)	0.3726 (0.0302)	0.7664 (0.2331)
	GDAS	0.6621 (0.0657)	0.4111 (0.1956)	0.6357 (0.3154)	0.7639 (0.2311)
	SETN	0.7108 (0.0765)	0.4107 (0.1991)	0.5206 (0.0412)	0.7672 (0.2278)
	Random	0.8112 (0.1886)	0.4313 (0.3671)	0.6452 (0.3517)	0.7659 (0.2032)
	TENAS	0.7937 (0.2063)	0.4353 (0.5645)	0.5754 (0.4246)	0.7559 (0.2403)
	DrNAS	0.7768 (0.2232)	0.4224 (0.5774)	0.6025 (0.3975)	0.7625 (0.2013)
	PC-DARTS	0.7647 (0.2353)	0.4273 (0.5726)	0.6040 (0.3960)	0.7612 (0.1726)
	SDARTS	0.7641 (0.2359)	0.4410 (0.5485)	0.6400 (0.3600)	0.7727 (0.0790)

Moreover, we observe that the NAS-searched architectures usually have lower overfitting levels than the human-designed architectures on all four datasets, which leads us to expect the robustness of the NAS-searched architectures against MIAs should be better than that of the human-designed ones, since previous work [47] have shown that a higher overfitting level of the target model usually leads to a better MIA performance. However, this conjecture conflicts with the observations of Pang et al.'s work [54], i.e., the NAS-searched architectures are more vulnerable to MIAs than the human-designed architectures, which motivates us to further explore the reason behind the conflicts and estimate the real privacy threats of various MIAs on the NAS-searched architectures. In fact, Pang et al. [54] only consider the label-only attack scenario in which the attacker has only access to the output labels of the target model, and their data sampling method for testing the MIA performance in their released code implementation[3] is actually biased to some data samples with extremely high confidence scores. To test our conjecture and comprehensively study the MIA threats on NAS-searched architectures with reliable and unbiased experimental results, we further evaluate the MIA performance with the aforementioned 5 attack settings on both the NAS-searched and the human-designed architectures.

Robustness Against Privacy Attacks. We compare their experimental results under aforementioned 5 different attack settings. The experimental results of ⟨Label-Only⟩, ⟨Black-Box, Shadow⟩, and ⟨White-Box, Shadow⟩ on the CIFAR10, CIFAR100 and STL10

[3] https://github.com/ain-soph/autovul/blob/main/projects/membership.py

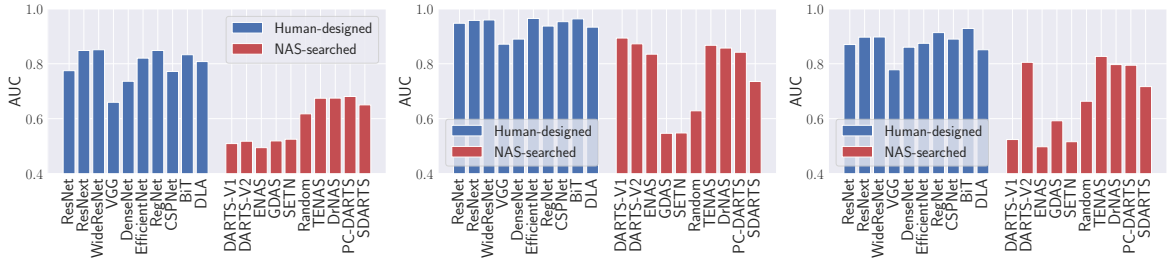

(a) CIFAR10 **(b) CIFAR100** **(c) STL10**

Figure 2: The performance of MIAs with the ⟨Label-Only⟩ setting on different datasets.

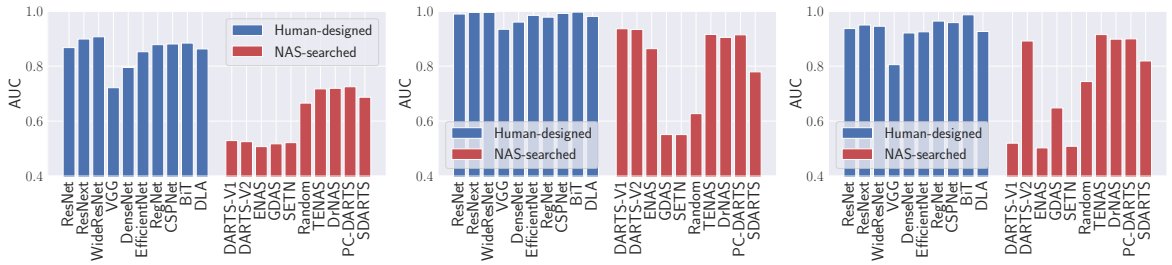

(a) CIFAR10 **(b) CIFAR100** **(c) STL10**

Figure 3: The performance of MIAs with the ⟨Black-Box, Shadow⟩ setting on different datasets.

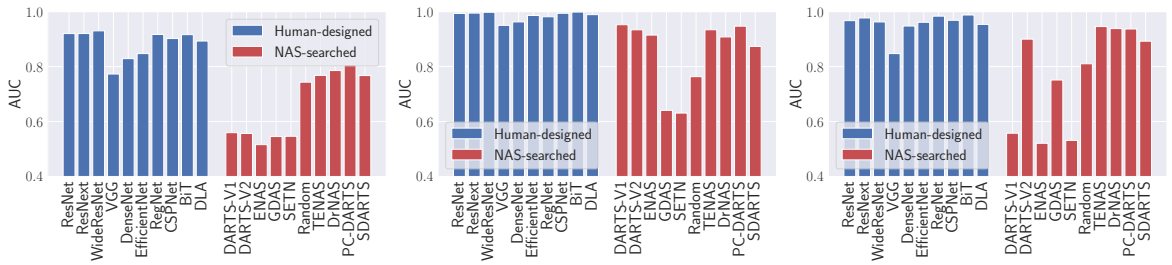

(a) CIFAR10 **(b) CIFAR100** **(c) STL10**

Figure 4: The performance of MIAs with the ⟨White-Box, Shadow⟩ setting on different datasets.

datasets are shown in Figure 2, Figure 3, and Figure 4 respectively. The results of the other two attack settings on these three datasets and all attack settings on the CelebA dataset can be found in Appendix B of our technical report [31].

First, we can observe that the MIAs usually have better performance under the white-box settings than the black-box settings. For instance, on the CIFAR10 dataset, the highest AUC score for MIAs on NAS architectures is around 0.81 under the ⟨White-Box, Shadow⟩ setting, while that under the ⟨Black-Box, Shadow⟩ is about 0.72, and that under the most constrained ⟨Label-Only⟩ settings is around 0.68. We believe that it is due to the abundant additional information (e.g., model weights, gradients) that the attackers extract from the white-box target model. Consequently, they can further manipulate such information to improve the performance of attacks. For example, the attacker can concatenate the gradients of hidden layers of the target white-box model with the output posteriors to serve as the input features for the attack model, which are more likely to enlarge the difference between members and non-members.

Second, given the same target dataset, the same target model tends to perform similarly in different attack settings. We can see that the architectures which obtain relatively high MIA AUC scores in one attack setting are still very likely to acquire relatively high MIA performance in other attack settings, and the histograms of different attack settings on the same dataset are quite similar. This interesting finding is also reasonable. Even though different attack settings might affect attack effectiveness, the majority of information needed by the attack is still offered by the output of the target model. Therefore, the same architecture tends to share similar robustness against MIAs regardless of the various attack settings.

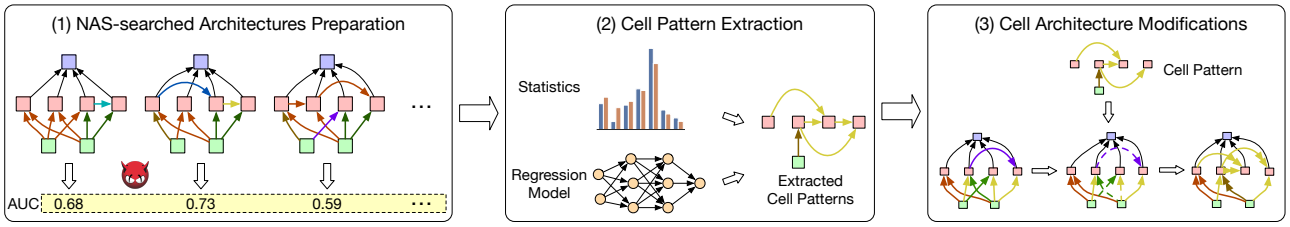

Figure 5: The overview of our framework exploring the correlation between the NAS architectures and MIA performance.

More importantly, we find that the NAS-searched architectures tend to be more robust against various MIAs than the manual ones, which means the latter faces more serious privacy threats than the former. For example, the red bars are usually lower than the blue bars in Figure 2. This further validates our aforementioned conjecture. However, we notice that our conclusion is contrary to the results from Pang et al. [54]. The root cause of such divergence is due to different sampling strategies used to sample member and non-member data. In our case, the distributions of member and non-member data have the same distribution as the original dataset. Pang et al. [54], however, sample data points with high classification confidence scores from the original dataset per their official implementation.[4] Their sampling strategy cannot guarantee the distributions of sampled member and non-member data have the same distribution as the original dataset.

4 ON EXPLORING PRIVACY-RELATED CELL PATTERNS

The empirical experimental results in Section 3 show that the NAS architectures are usually more robust against MIAs; however, different NAS architectures still pose different levels of robustness against MIAs. Some NAS architectures (e.g., DARTS-V2) even appear to be more vulnerable to MIAs than the human-designed VGG on the STL10 dataset. Therefore, in this section, we aim to understand the relationship between the robustness against MIAs and the NAS architectures. Concretely, we seek to address the following questions: (1) *What are the common structures among existing NAS architectures which might impact MIAs?* (2) *Can we find some existing architectural patterns to decrease the MIA risks of the NAS architectures when building NAS?* and (3) *If we do, can we maintain the model performance while decreasing the MIA risks?*

4.1 Overview

Figure 5 illustrates the overall framework for analyzing and evaluating the correlation between the cell patterns and robustness against MIAs of NAS architectures, which consists of three steps.

- **NAS-searched Architecture Preparation.** We first collect a large number of NAS-searched architectures with good model utility and evaluate the corresponding MIA performance on them for subsequent analysis.
- **Cell Pattern Extraction.** We then look deep into the internal cell structures of these NAS-searched architectures and propose a new method to extract common cell patterns that can promote or demote the MIA performance.
- **Cell Architecture Modification.** Finally, we use the extracted cell patterns to modify the internal cell structure of the target architecture to promote or demote the MIA performance on it.

4.2 NAS-searched Architectures Preparation

It is infeasible for us to train thousands of NAS-searched architectures from scratch. Instead, we use NAS-Bench-301 [66], a large scale open-sourced benchmark dataset that contains 59,328 full-trained NAS-searched architectures identified by 17 representative NAS algorithms in a huge DARTS search space (i.e., 10^{18} possible architectures) on the CIFAR10 dataset. We drop the redundant architectures which appear multiple times in NAS-Bench-301 and obtain a collection of NAS-searched architectures consisting of 53,558 unique architectures.

As we can see in Table 1, NAS-searched architectures with high test accuracy tend to have low overfitting levels. Their cell patterns are more likely to have better robustness against MIAs while maintaining good model performance at the same time. Besides, in the real world, the end users tend to choose architectures with high model performance. As such, we select the top 5% (i.e., 2,678) architectures with the highest test accuracy scores from NAS-Bench-301. We then evaluate the MIA effectiveness under the most powerful attack setting, i.e., ⟨White-Box, Partial⟩ (see Section 3.2 for details) for each sampled architecture to constitute an *Architecture-to-MIA* dataset containing the well-performed architectures and their corresponding MIA AUC scores. The MIA AUC scores in this new dataset range from 0.7311 to 0.8773. We group the architectures with MIA AUC scores higher than 0.84 and lower than 0.78 into *high* (denoted as $\mathcal{A}_{\text{high}}$) and *low* (denoted as $\mathcal{A}_{\text{low}}$) MIA categories. In total, we have 297 $\mathcal{A}_{\text{high}}$ and 303 $\mathcal{A}_{\text{low}}$ NAS-searched architectures for our cell pattern analysis.

4.3 Cell Pattern Extraction

To get a deeper understanding of the cell structures preferred by the robust or vulnerable NAS architectures, we look into the internal cell structures and try to extract some common cell patterns for specific objectives (e.g., demote the performance of MIAs). Here we take the $\mathcal{A}_{\text{high}}$ and $\mathcal{A}_{\text{low}}$ architectures for cell pattern extraction since they are the most vulnerable and robust architectures respectively in our constructed *Architecture-to-MIA* dataset.

Operation Distributions. We first analyze the distributions of operations in the normal and reduction cells of these two types of architectures. We have an interesting finding that the convolution

[4] Line 52 in https://github.com/ain-soph/autovul/blob/main/projects/membership.py

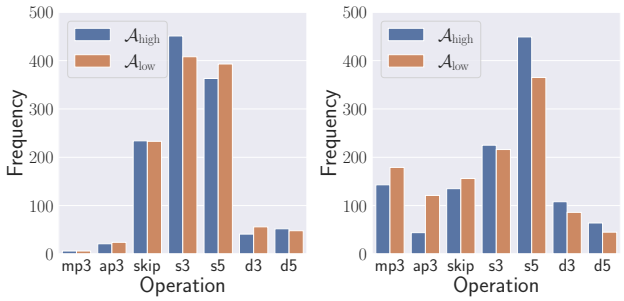

(a) Normal **(b) Reduction**

Figure 6: Distributions of various operations in the normal and reduction cells of both $\mathcal{A}_{\text{high}}$ and $\mathcal{A}_{\text{low}}$ architectures.

operations seem critical for model performance while the pooling operations are preferred to mitigate MIAs. As shown in Figure 6, the *separable convolutions* and *skip connections* occupy the majority of operations in both normal and reduction cells regardless of the architecture type, which means that these operations are critical to model performance on original tasks. However, we find some changes in the distribution of operations when the architecture type moves from $\mathcal{A}_{\text{high}}$ to $\mathcal{A}_{\text{low}}$, especially for specific operations in the reduction cells. Furthermore, according to previous observations in [70], the reduction cell has a relatively small impact on the overall model performance which is dominated by normal cells. And both the $\mathcal{A}_{\text{high}}$ and $\mathcal{A}_{\text{low}}$ architectures sampled by us have good model performance, so it is expected that the difference between the operation distributions in the normal cells of these two types of architectures is relatively small. Therefore, we can observe that the change of the operation distributions in the reduction cells is more obvious than that in the normal cells. The frequency of the average pooling 3×3 operation ap3 increases drastically by 175% when the architecture type changes from $\mathcal{A}_{\text{high}}$ to $\mathcal{A}_{\text{low}}$. In general, as for the reduction cells, the convolution operations are preferred by the $\mathcal{A}_{\text{high}}$ architectures, while the pooling operations (especially the average pooling operation) are favored by the $\mathcal{A}_{\text{low}}$ architectures. When it comes to the normal cells, even though the operation distributions of both the $\mathcal{A}_{\text{high}}$ and $\mathcal{A}_{\text{low}}$ architectures are quite similar to retain model performance, we can still observe that the separable convolution 3×3 operation s3 is particularly favored by the $\mathcal{A}_{\text{high}}$ architectures.

Operation Importance. The information obtained from merely the distributions of various operations is far from enough to represent the common cell patterns among the well-performed architectures since the NAS architectures might comply with specific topologies to guarantee model performance. Therefore, we go even further to extract specific cell patterns containing both the topology and operation information. To construct a cell pattern with specific edges, we need to determine the importance of each edge. Following similar strategy in [70], we use *Operation Importance* (OI) to measure the impact of specific operations with specific edges. For a NAS cell architecture α, the directed edge $e_{(i,j)}$ starts from node i to node j, we assume that the edge $e_{(i,j)}$ is assigned with operation o_t, then the OI metric for o_t on edge $e_{(i,j)}$ is computed as follows:

$$\text{OI}(\alpha, e_{(i,j)} := o_t) = \frac{\sum_{k=1}^{|\mathcal{N}(\alpha, e_{(i,j)} := o_t)|} f(\alpha_k)}{|\mathcal{N}(\alpha, e_{(i,j)} := o_t)|} - f(\alpha), \quad (1)$$

where $f(\alpha)$ stands for the MIA AUC score of NAS cell architecture α and $\mathcal{N}(\alpha, e_{(i,j)} := o_t)$ represents the neighbor cell set of the original cell architecture α.

We regard a cell as a neighbor cell of the original cell architecture α with operation o_t on edge $e_{(i,j)}$ when we either replace operation o_t with another operation $o_p (o_p \neq o_t)$ or change the input node i of edge $e_{(i,j)}$ to another preceding node $q (q \neq i)$ in the original cell architecture α to obtain the current cell. OI compares the average MIA performance on the neighbor cells with that on the original cell architecture. A positive value indicates that the current operation in the current edge can mitigate the MIA threats, while a negative value means that the current operation can contribute to MIA performance. Therefore, the attacker prefers the operation-assigned edge with a small negative value, while the defender favors an edge with a large positive value. Note that the MIA evaluation on one cell can be time-consuming (usually takes about 2 hours in our experiments). Even if we consider only modifying a single edge in a cell, it may affect multiple neighbor cells. In turn, iteratively evaluating each neighbor cell after re-training from scratch would be computationally prohibitive when there are many original cells for analysis.

GIN-based Regression Model. To speed up the computation process and make this method feasible in reality, we use the aforementioned *Architecture-to-MIA* dataset to train a regression model to directly predict the MIA performance when the cell architecture is given. The core idea is to build a regression model to achieve the speed-up. The input of the regression model is the architecture, and the output data is its corresponding predicted MIA AUC score. Here we randomly divide the *Architecture-to-MIA* dataset into three parts with 80%, 10%, and 10% as training, validation, and testing datasets, respectively. We test multiple regression methods (i.e., SVR [19], Random Forest [27], LGBoost [35], XGBoost [9], BANANAS [75], and GIN [77]) to select the model which can best fit the relationship between the NAS architectures and MIA AUC scores. The experiments use the same parameter settings for these regression models as the publicly available implementation of NAS-Bench-301.[5]

Table 2: Performance of different regression models trained on the constructed dataset.

Model	Metrics	
	R^2	SpearmanR
SVR	0.1097	0.3055
Random Forest	0.1021	0.3155
LGBoost	0.0718	0.2783
XGBoost	**0.1332**	0.3394
BANANAS	-0.0586	0.2003
GIN	0.0788	**0.3751**

The experimental results are show in Table 2. We use two metrics (i.e., R^2 and SpearmanR) to estimate the performance of different regression models. R^2(coefficient of determination) measures how well the observed results are replicated by the model according

[5]https://github.com/automl/nasbench301.git

to the proportion of the outcome variance successfully explained by the model. SpearmanR (Spearman rank-order correlation coefficient) measures the monotonicity of the relationship between the two datasets (i.e., the ground-truth AUC scores and the predicted AUC scores in our experiments). Higher scores of R^2 are preferred and the best possible value of it is 1.0, while scores with higher absolute values are favored for SpearmanR whose best score is +1/-1. We can observe that the XGBoost model obtains the best R^2 score while the GIN model achieves the best SpearmanR score. Additionally, since the architecture of a NAS cell can be represented as a DAG, and GIN model is a powerful variation of Graph Neural Networks (GNNs) which can learn plentiful information from the architectures of graph data and have surpassed many traditional techniques on graph tasks, it is very reasonable to use GIN in this scenario. As a result, we choose the GIN model as the regression model for further experiments and analysis. Note that we use this GIN-based regression model $\widetilde{f}$ to replace f in Equation 1. In turn, we can immediately estimate the MIA AUC score after we get one specific cell architecture.

Cell Pattern Categories. According to the goals of different cell patterns, we divide the cell patterns into two categories, i.e., MIA *promotion* and MIA *demotion*, where the MIA promotion cell patterns aim to improve the performance of MIAs while the MIA demotion cell patterns attempt to mitigate MIA threats. Take the MIA demotion cell patterns for example, we prefer to choose the edges with a large positive value. Additionally, to accumulate the effectiveness of every single edge in the cell pattern, when constructing the cell pattern one by one edge, we ensure that the selected new edge is adjacent to the current cell pattern (i.e., having nodes in common). In this way, all selected edges are connected as a whole graph. Besides, we make sure that the cell patterns comply with the DARTS cell construction rule, e.g., each intermediate node has at most two input edges.

Extraction Strategy. The extraction strategy is shown in Algorithm 1. To focus on the operation-signed edges which are more common among sampled architectures, we only consider and compare the OI scores of those edges appearing more than 14 times in the candidate edge set $\mathcal{E}$ when we analyze the cell patterns for the normal or reduction cells of $\mathcal{A}_{\text{high}}$ or $\mathcal{A}_{\text{low}}$ architectures. Our extraction strategy consists of 4 steps:

- **Initialization.** We separately compute the operation importance for the normal and reduction cells in $\mathcal{A}_{\text{high}}$ or $\mathcal{A}_{\text{low}}$ architectures, and follow Line 1-7 to prepare for the extraction.
- **Edge Constraint Checking.** We check the number of edges in the current cell pattern in Line 8 and will terminate the extraction process in advance using Line 24 if no more new edge is successfully added to the current cell pattern graph.
- **Construction Rule Checking.** We check whether the current edge is adjacent to the current cell pattern graph and also comply with the rule in the DARTS search space using Line 14.
- **Operation Importance Checking.** We check whether the operation importance score of the current edge meets our requirements using Line 15 and will update the current cell pattern and other data recorders using Line 16-22 if this edge is successfully added.

Algorithm 1: Cell Pattern Extraction

Input: Candidate edge set $\mathcal{E}$, maximum number of edges in the cell pattern L, demotion flag δ
Output: Cell pattern graph G_p

1 Initialize the in-degree dictionary D_{in} with 0 for each node;
2 Initialize the existing cell pattern graph G_p, edge topology set E_p and node set V_p as empty sets;
3 **if** δ **then**
4 Sort $\mathcal{E}$ in descending order according to OI scores;
5 **else**
6 Sort $\mathcal{E}$ in ascending order according to OI scores;
7 Add the input node of the first edge $\mathcal{E}_1$ in $\mathcal{E}$ to V_p;
8 **while** $|G_p| < L$ **do**
9 $\epsilon \leftarrow$ False;
10 $N \leftarrow |\mathcal{E}|$;
11 **for** $i \leftarrow 1$ **to** N **do**
  // Start node u, end node v, operation o
12 $(u, v, o) \leftarrow \mathcal{E}_i$;
13 $\tau \leftarrow \text{OI}((u, v, o))$;
14 **if** $(u \in V_p$ **or** $v \in V_p)$ **and** $(u, v) \notin E_p$ **and** $D_{\text{in}}[v] < 2$ **then**
15 **if** $(\delta$ **and** $\tau > 0)$ **or** (**not** δ **and** $\tau < 0)$ **then**
16 $G_p \leftarrow G_p \cup (u, v, o)$;
17 $E_p \leftarrow E_p \cup (u, v)$;
18 $V_p \leftarrow V_p \cup \{u, v\}$;
19 $D_{\text{in}}[v] \leftarrow D_{\text{in}}[v] + 1$;
20 $\mathcal{E} \leftarrow \mathcal{E} \setminus (u, v, o)$;
21 $\epsilon \leftarrow$ True;
22 **break**
23 **if not** ϵ **then**
24 **break**

Note that the NAS cell architectures in the NAS-Bench-301 dataset have 4 intermediate nodes and up to 8 edges in a cell can be modified; thus, we thereby set $L = 8$. We set the demotion flag δ to "True" to search for the MIA demotion cell patterns, and "False" otherwise to search for the MIA promotion cell patterns.

4.4 Cell Architecture Modifications

Through the above efforts, we can extract the cell patterns from the *Architecture-to-MIA* dataset. Based on these cell patterns, we could go further to modify the internal cell structure of the target architecture to promote or demote MIA performance on it.

Extracted Patterns. Figure 7 illustrates the extracted patterns, including both MIA demotion and promotion cell patterns extracted from normal cells and reductions, respectively. We have several interesting findings according to the extracted cell patterns.

- First, separable convolution and dilated separable convolution operations are preferred by the normal cells in both the MIA demotion and promotion cell patterns. As we have discussed before, this is because the model performance is mainly determined by the normal cells and some common operations are necessary for maintaining good model performance.

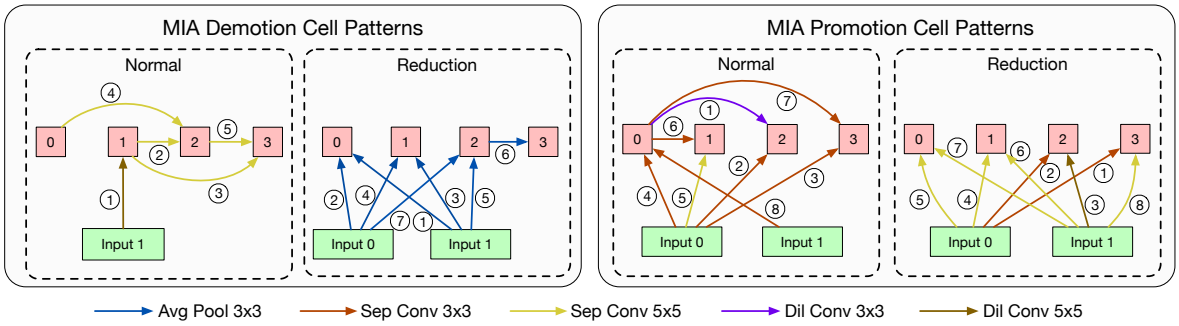

Figure 7: The extracted cell patterns for both MIA demotion and promotion on both normal and reduction cells. The numbers in circles near edges indicate the order in which the corresponding edges were selected for the cell pattern in the cell.

- Second, reduction cells prefer average pooling operations when demoting MIAs but favor convolution operations for MIA promotion. This is also consistent with our findings in the operation distributions of different architectures (see Section 4.3).
- Third, the edges in the MIA demotion cell pattern on normal cells are mainly connected between intermediate nodes, while those of other cell patterns are mainly connected to the input nodes. We speculate the reason is that MIA demotion cell patterns use this way to impede direct information transmission for normal cells. According to the statistical results in Figure 6 and the extracted MIA promotion cell patterns in Figure 7, convolution operations seem to be beneficial to MIAs but the normal cells have to use them to retain good model performance even in the MIA demotion cell pattern. To weaken the negative impact of convolutions on privacy, the MIA demotion cell patterns prefer to place these operations in some positions not directly connected to the input nodes to avoid the information with high fidelity being leaked through these operations. On the contrary, max-pooling operations seem to be helpful to mitigate MIAs, so they are mainly directly connected between the input nodes and the intermediate nodes to protect the original information. As for the MIA promotion cell patterns, convolution operations are largely connected to the input nodes to facilitate extracting information with high fidelity.

Cell Architecture Modifications. Our architectural modifications to the target architectures work as follows. First, according to our goal (e.g., promoting MIA performance on the target architecture) and the constraints on our modifications, we constitute corresponding cell patterns from Figure 7 to guide modifications on specific types of cells. For example, when we want to achieve MIA demotion goal, and we are limited to perturb only the normal cell architectures and determine the structure in a cell for up to 4 edges, we select 4 edges from the MIA demotion cell pattern on normal cells following the sequence of the corresponding circled numbers (shown in the left side of Figure 7). We then get the required cell pattern as shown in the upper part of Figure 8.

Second, upon obtaining the cell pattern, we compare the internal structure of both the cell pattern and the normal cell of the target architecture. If an edge $e_{(i,j)}$ with the assigned operation o_t in the cell pattern does not exist in the target normal cell, we replace another existing edge $e_{(k,j)}$ in the target normal cell with the same

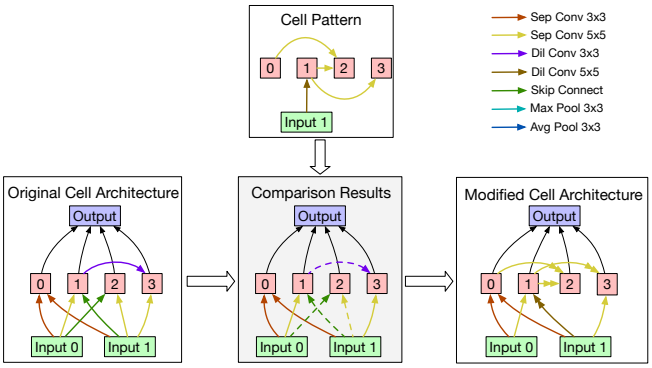

Figure 8: An example of cell architecture modifications based on the cell pattern. The arrows with dashed lines represent candidate edges to be replaced, while the filled double arrows with solid lines stand for the newly added edges as modifications.

end node of $e_{(i,j)}$. If there already exists the edge $e_{(i,j)}$ but with a different operation $o_{t'}$ ($o_{t'} \neq o_t$) in the target normal cell, we simply alter its operation $o_{t'}$ to o_t later. The arrows with dashed lines in Figure 8 represent the original edges ready to be changed.

Finally, we make the modifications to the replacement candidate edges, and replace these edges with the corresponding edges in the cell pattern. The filled double arrows with solid lines in Figure 8 stand for the newly added edges to the target normal cell. After taking these three steps, the target normal cell is successfully modified to comply with the cell pattern.

5 CELL PATTERN EVALUATION

5.1 Experimental Setup

Cell Pattern Modification Configuration. We evaluate three categories of cell modifications, namely *Only-Reduction*, *Only-Normal* and *Dual* modifications. *Only-Reduction* modifications are exclusively made to the reduction cell of the target NAS architecture. Similarly, *Only-Normal* modifications are made only to the normal cell of the target NAS architecture. *Dual* modifications indicate that the modifications are made to both reduce and normal cells of

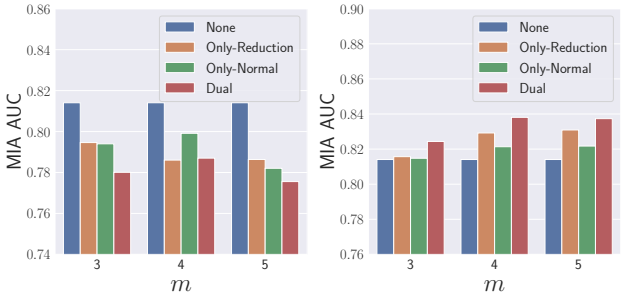

(a) Demotion (b) Promotion

Figure 9: MIA performance with various cell patterns under different cell pattern constraints. "None" means no architectural modification is applied to the target architectures.

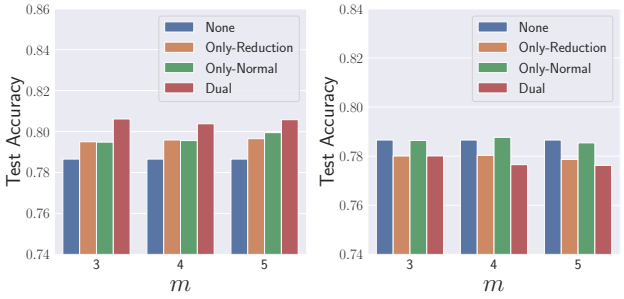

(a) Demotion (b) Promotion

Figure 10: Model utility with various cell patterns under different cell pattern constraint values. "None" means no architectural modifications are applied to the target architectures.

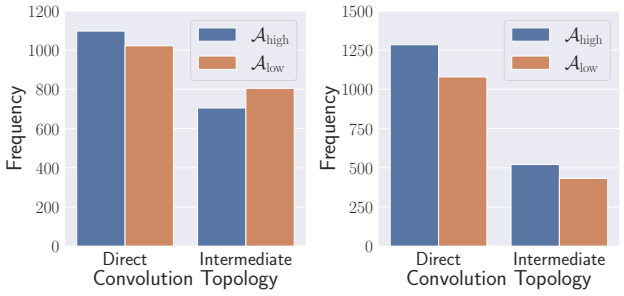

(a) Normal (b) Reduction

Figure 11: Distributions of convolutions with two types of topology in the normal and reduction cells of both $\mathcal{A}_{\text{high}}$ and $\mathcal{A}_{\text{low}}$ architectures.

the target architecture. For all these modifications, we use the cell patterns identified in Figure 7.

Modification Budget. Note that the cell patterns extracted in Figure 7 tend to include as many edges as possible to either demote or promote MIA performance. However, in the real world, we may not be allowed to modify that many edges in a cell since it would significantly limit the space searchable by various NAS algorithms. That is, the more edges determined by the cell patterns, the fewer edges useable by the NAS algorithm, since the overall amount of edges is fixed. For example, we have 8 edges in total for the DARTS cell (see Figure 1). If the cell pattern has 6 edges, a NAS algorithm has only 2 edges to search. We thereby set a modification budget m to limit the number of edges we can select from one cell pattern. In turn, our final cell patterns used in our experiments contain at most the first m edges from the full cell patterns as shown in Figure 7. We use $m = \{3, 4, 5\}$ to evaluate the effectiveness of cell pattern modifications.

Runtime Configuration. Unless otherwise mentioned, we randomly sample 10 NAS-searched architecture instances from our *Architecture-to-MIA* dataset as the target NAS architectures and average their results. We set $m = 4$ and conduct the experiments on the CIFAR10 dataset by default.

5.2 Effectiveness of the Cell Patterns

We evaluate the MIA performance under the ⟨White-Box, Partial⟩ setting on the CIFAR10 dataset. The experimental results for both MIA performance and model utility (i.e., the test performance on the testing dataset for the target model) are shown in Figure 9 and Figure 10 respectively.

The first observation is that our cell patterns can successfully demote or promote MIAs as intended in all cases. Take Only-Reduction modification and modification budget $m = 4$ for instance, the average MIA AUC score of the target architectures drops from 0.8141 to 0.7861. Though a small MIA AUC score decrease from the absolute value perspective, however, such drop can reduce the privacy risks since the real-world models usually requires a huge amount of user data to train.

Our second observation is that it is relatively easier to demote MIA AUC scores of NAS-searched architectures than to promote them. Our hypothesis is that the convolution topology difference between $\mathcal{A}_{\text{low}}$ and $\mathcal{A}_{\text{high}}$ may contribute to this phenomenon. To this end, we further count the number of the convolution operations with two different topologies — the *direct* topology where the convolution operations connect to the input nodes and the *intermediate* topology where the convolution operations connect two intermediate nodes. For instance, in the MIA demotion cell pattern on the reduction cells in Figure 7, the edge marked with the circled number 6 stands for the intermediate topology, while all the other edges belong to the direct topology. The statistical results for convolution topologies are shown in Figure 11. As we can see in Figure 11, the frequency of *direct* convolution topology is always higher than that of the *intermediate* convolutions. And also, the normal cells in the $\mathcal{A}_{\text{low}}$ architectures contain more *intermediate* convolution topology than those of the $\mathcal{A}_{\text{high}}$ architectures. Recall that Section 4.4 shows that the MIA promotion cell pattern on both normal and reduction cells contains many direct convolutions, while the MIA demotion cell patterns on both the normal and reduction cells contain few *direct* convolutions. Adding more direct convolutions (i.e., promotion) to $\mathcal{A}_{\text{high}}$ and $\mathcal{A}_{\text{low}}$ would have less impact on MIA performance due to the fact that the frequency of *direct* convolution topology is always high in both cases. On the other hand, reducing direct convolutions (i.e., demotion) is more

effective in decreasing the MIA AUC scores, hence more evident in $\mathcal{A}_{\text{high}}$ and $\mathcal{A}_{\text{low}}$.

Our third observation is that cell patterns with more edges tend to have a larger impact on MIA robustness. For example, when we increase the modification budget m from 3 to 5 in Figure 9b, the MIA performance of the target architectures under the Only-Normal MIA promotion modifications ascend from 0.8148 to 0.8217. Note that, even when the cell patterns have merely $m = 3$ edges, the Only-Normal MIA demotion modifications can still effectively decrease the MIA performance from 0.8141 to 0.7940 in Figure 9a.

Besides, in the MIA demotion scenario, the model utility is even improved after the robustness of the target architecture has been strengthened, which is a desired and satisfying result. The reason behind this phenomenon is that the MIA performance is correlated with the overfitting level of the target model [47]. After we apply the MIA demotion cell patterns, the overfitting level of the target model decreases. The reduced overfitting level helps the target model generalize better and promote the model utility at the test time. For instance, after the Only-Reduction MIA demotion modifications with $m = 4$, the MIA performance in Figure 9a drops from 0.8141 to 0.7861, while the corresponding test accuracy in Figure 10a increases from 0.7866 to 0.7959. The overfitting level of the target model drops from 0.2134 to 0.2041 in this case. Note that, Only-Normal modifications usually have a relatively small impact on the model performance of the target architectures. As we have discussed in Section 4.4, the cell patterns on normal cells have tried to mitigate the side effects on model performance and mainly contain convolution operations.

Finally, Dual modifications usually have the largest impact on the model utility and MIA robustness. For instance, when the modification budget limited to $m = 3$ in Figure 9a, Only-Normal and Only-Reduction MIA demotion modifications can demote the MIA AUC score of the target architectures from 0.8141 to 0.7940 and 0.7946 respectively, while Dual modifications can further reduce the MIA AUC score to 0.7801. At the same time, the test accuracy of the architecture in Figure 10a is improved from 0.7866 to 0.7948, 0.7950, and 0.8061 respectively for Only-Normal, Only-Reduction, and Dual modifications. Note that, we also conduct ablation studies on the impact of the number of cells and the number of intermediate nodes in Appendix D of [31] to get a deeper understanding of the cell patterns. Particularly, we find that deeper networks tend to be more robust while wider networks tend to be more vulnerable to MIAs.

5.3 Loss Contour Analysis

To further investigate the impact of MIA demotion or promotion modifications, we leverage loss contour of the target architecture to understand how those architectures behave after the modifications have been made. We sample one architecture already evaluated in Section 5.2, and plot its training loss contour with regarding to model weight parameters changes using the code implementation[6] of Li et al.'s work [40]. Both MIA demotion and promotion modifications are Only-Reduction ones, and the experiments are conducted on the CIFAR10 dataset. The loss contours are shown in Figure 12.

[6]https://github.com/tomgoldstein/loss-landscape

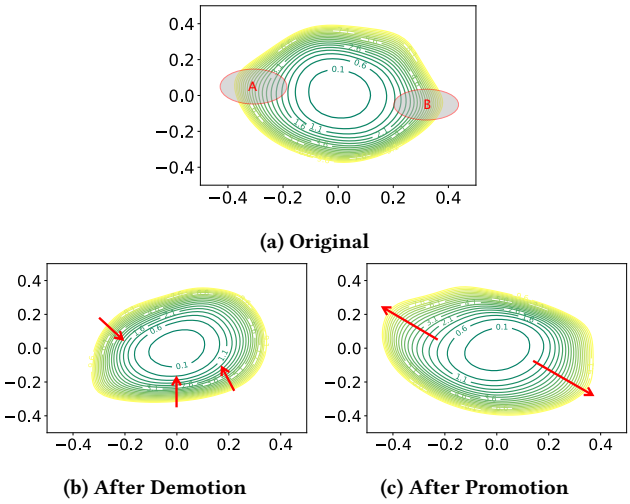

(a) Original

(b) After Demotion

(c) After Promotion

Figure 12: The contours before and after MIA demotion or promotion modifications of the target architecture.

The circled gray areas A and B in Figure 12a represent the "trustworthy" areas for MIAs in the loss contour of the original target architecture. We notice that the loss contour tends to be sparse in A and B. It means that small perturbations (e.g., training randomness) on the model weights do not affect the loss values of the training dataset much, offering "trustworthy" posteriors of training members for the attacker to discriminate those of non-members. In Figure 12b and Figure 12c, we use arrows to demonstrate the changing trends of the loss contours near the trustworthy areas compared to the original loss contour after the corresponding modifications. We observe that the loss contour near the trustworthy areas of the original loss contour tends to be denser after the MIA demotion modifications. In comparison, the trustworthy areas tend to be sparser after the MIA promotion modifications. The potential reason is that, when the loss contour in these areas becomes denser, little perturbations on the model weights may make the loss values change significantly. The consequence is that many data samples are pushed close to the decision boundary of the current model. In this way, the attacker can only get less confident posteriors from the target model, which hinders the performance of MIAs. And both the MIA demotion and promotion modifications affect the robustness against MIAs by changing the shapes of the loss contour of the target model. Further, our cell patterns have little impact on the model performance, so the overall flatness of the loss contour of the target model has not been changed much.

5.4 Transferability

Our cell patterns are extracted based on the MIA evaluation results with the most knowledgeable ⟨White-Box, Partial⟩ attack setting on the sampled architectures from NAS-Bench-301, a NAS architecture dataset searched in the DARTS search space on the CIFAR10 dataset. Here we want to check whether our cell patterns can transfer to other scenarios.

Transferability among Different Attack Settings. Our cell patterns are extracted based on the MIA evaluation results with the

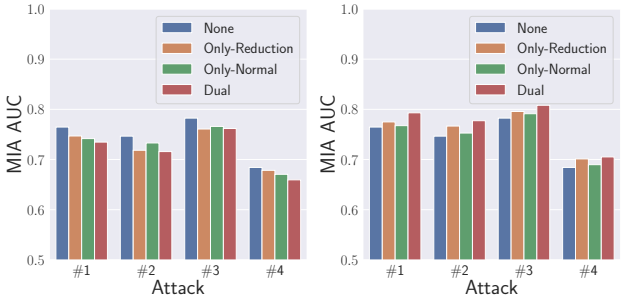

(a) Demotion (b) Promotion

Figure 13: Transferring MIA performance of the cell patterns on various MIAs. #1, #2, #3, and #4 represent the ⟨Black-Box, Shadow⟩, ⟨Black-Box, Partial⟩, ⟨White-Box, Shadow⟩ and ⟨Label-Only⟩ attack settings respectively.

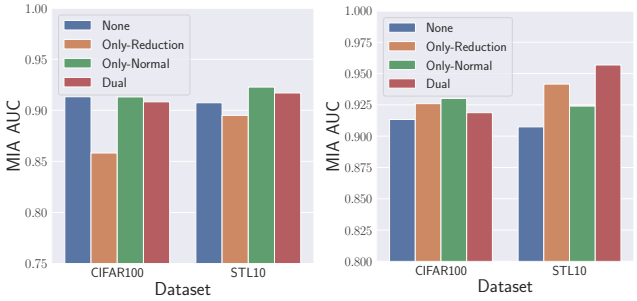

(a) Demotion (b) Promotion

Figure 14: Transferring MIA performance for the cell patterns on different datasets.

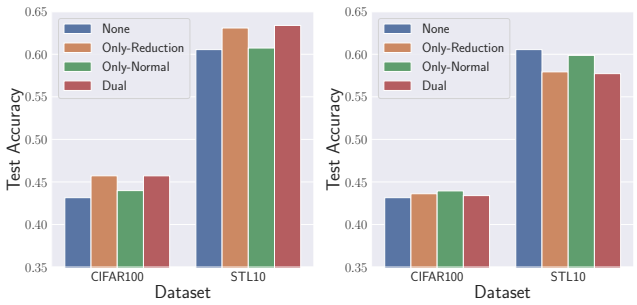

(a) Demotion (b) Promotion

Figure 15: Model utility under the transferred cell patterns on different datasets.

⟨White-Box, Partial⟩ setting, here we would like to see whether our cell patterns also work for other attacks with different attack settings. We change the attack setting for MIAs and re-evaluate the target architectures before and after the MIA demotion and promotion modifications, and the results are shown in Figure 13. We could see that our cell patterns are still effective for all these attacks in all cases, which demonstrates the high transferability of our cell patterns.

Transferability among Different Datasets. Our cell patterns are extracted from the architectures searched on the CIFAR10 dataset, here we want to explore whether our cell patterns are also effective on other datasets. Here we apply our cell patterns to 4 architectures using the last four NAS algorithms in Section 3.2 and searched on CIFAR100, STL10 and CelebA datasets respectively, and evaluate the MIA performance and model utility before and after the architectural modifications.

The experimental results on the CIFAR100 and STL10 datasets are shown in Figure 14 and Figure 15. We defer the evaluation results and corresponding analysis on the CelebA dataset to Appendix E of [31]. It is observed that our cell patterns can still achieve the desired MIA demotion or promotion goals in most cases, which means our cell patterns are also transferable to different datasets. Besides, we can observe that the Only-Reduction modifications tend to have the best performance, while the Only-Normal modifications are inferior to the former. The possible reason is that the model performance of cell-based NAS architectures is mainly determined by the normal cells [70], and the architectures searched on different datasets tend to have different normal cell architectures, which hinders the transferring of the cell patterns on normal cells.

Note that, since our cell patterns are extracted from the DARTS search space, we also test the transferring effectiveness of our cell patterns in the NAS-Bench-201 search space in Appendix F of our technical report [31]. And it is observed that our cell patterns can still partially transfer to the NAS-Bench-201 search space.

5.5 Enhancing Existing Defenses

Existing defenses against MIAs mainly focus on improving the robustness of the target model by masking confidence scores [33, 43, 64], regularization [34, 51, 64], or differential privacy [6, 32, 63], etc. In contrast, our MIA demotion cell patterns are performed in the model architecture design phase and are different from previous defense strategies. Naturally, we wonder if our approach can not only improve the model robustness against MIAs by itself but also complement existing defense techniques when using together?

To this end, we further conduct experiments to estimate whether our MIA demotion cell patterns can enhance existing defense strategies. We choose three representative defense methods which could be applied on both black-box and white-box MIA settings, i.e., data augmentation (DA) [34], label smoothing (LS) [68], and differential privacy (DP) [21]. DA increases the number of training samples by exerting slight modifications to the original data samples and can decrease the overfitting level. LS is a regularization method to mitigate the overconfidence of the target model. DP adds well-calibrated perturbations to the training process of the target model.

The experimental results are shown in Figure 16. We can see that, our MIA demotion cell patterns can successfully enhance the performance of these existing defense strategies in all cases in Figure 16a with a slight impact on the model utility in Figure 16b. To further validate whether our cell patterns can enhance existing defenses even when transferring to other attack settings, we conduct the transferability experiments of other attack settings under defense in Appendix G of our technical report [31]. Overall, our

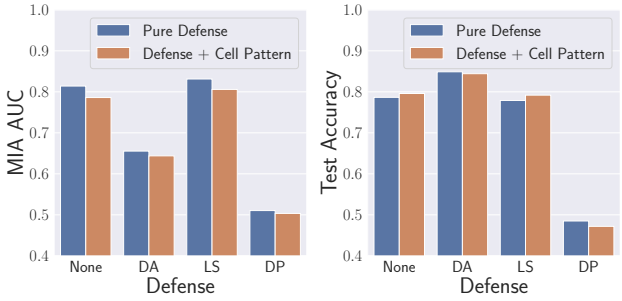

(a) MIA Performance **(b) Model Utility**

Figure 16: MIA effectiveness and model utility under defenses.

MIA demotion cell patterns are shown to be able to promote the effectiveness of the existing defense methods in almost all cases for various attack settings, setting a safer lower bound for the existing defense strategies.

5.6 Guidelines for Improving Robustness

According to previous experimental results and analysis, we can conclude some general and meaningful guidelines for designing and using more robust cell-based architectures against MIAs:

(1) *Convolution operations* are important for model performance; however, the architectures with relatively high MIA performance tend to have more convolution operations than others. Therefore, we should use moderate number of convolution operations to strike a tradeoff between model utility and robustness.
(2) Use less convolutions directly connected to the input nodes.
(3) If more convolution operations are indeed necessary, refer to the second guideline. In this case, constructing a deeper network architecture is recommended.
(4) Limit the width of the cell, which usually can be easily done by limiting the number of intermediate nodes in a cell.

6 RELATED WORK

Membership Inference Attack. Membership inference attack (MIA) is a privacy attack method to infer whether a given data sample is present in the training dataset of the target machine learning models [29]. It is firstly proposed by Shokri et al. [64] and has developed many variants for various scenarios. Shokri et al. [64] use multiple shadow models trained on the shadow dataset to mimic the behavior of the target model, then train an attack model with the output posteriors of the shadow models to predict if a sample is used to train the target model. Salem et al. [62] relax the key assumptions of Shokri et al. [64] and propose model and data independent attack methods to effectively predict memberships under various attack settings. Since then, membership inference attacks have been applied to many domains (e.g., computer vision [43, 52, 80], graph data [26], unlearning systems [7, 8], and even recommender system [83]) and different target models (e.g., classification model [7], generative model [6], embedding model [45] and multi-exit model [42]) with different attack techniques. To mitigate the privacy threats of membership inference attacks, many defense strategies have been proposed, including confidence masking [43], regularization [51, 64], differential privacy [6, 20, 74, 84, 85] and knowledge distillation [63]. Our MIA demotion cell patterns utilize the inherent robustness of specific structures to mitigate the vulnerability of the target model. Those patterns are model-agnostic and complementary to existing defense work to further enhance the robustness of the target model.

Security and Privacy of NAS. The security and privacy threats of NAS architectures have not been well-studied and previous research also leads to contradictory findings. Guo et al. [24] reveal several insightful observations (e.g., convolution operations to direct connection edge, densely connected patterns, etc.) that can improve the adversarial robustness of NAS-searched architectures. Their research leads to some recent research work improving the robustness of NAS-searched architectures against adversarial perturbations to improve the accuracy of those models [15, 41]. On the other hand, Oymak et al. [53] demonstrate that the train-validation accuracy gap decreases rapidly when the validation data is mildly large (i.e., achieving a low overfitting level), which in turn makes NAS-searched architectures robust against MIAs. Yet, in the most recent work, Pang et al. [54] show that NAS architectures are more vulnerable to existing security and privacy attacks than the human-designed architectures including MIAs. However, their research only evaluates limited scenarios for these attacks. In our work, we conduct a comprehensive measurement study of the privacy risks of NAS architectures. We eliminate the experimental bias introduced in the previous research and compare the MIA performance on both NAS-searched architectures and human-designed architectures using all known MIA attack scenarios. We find that NAS-searched architectures are generally more robust against MIAs but such robustness varies from architecture to architecture.

7 CONCLUSION

In this paper, we conduct comprehensive measurement experiments for MIAs on both NAS-searched and human-designed architectures, and show that NAS-searched architectures tend to be more robust against MIAs. Furthermore, to analyze the hidden cell patterns affecting the robustness against MIAs, we design a general framework to extract the cell patterns based on the evaluation results on sampled NAS architectures. We use this framework to extract both MIA demotion and promotion cell patterns from existing well-performed NAS architectures. The experimental results show that our cell patterns can successfully demote or promote the MIA performance on the target architectures and can transfer to various scenarios. Additionally, our MIA demotion cell patterns are complementary to existing defense techniques and can further enhance the performance of the latter. Finally, we offer some guidelines to design more robust NAS architectures against MIAs in the future.

ACKNOWLEDGMENTS

We thank our shepherd Xi He and all anonymous reviewers for their constructive comments. This work is partially funded by the Helmholtz Association within the project "Trustworthy Federated Data Analytics" (TFDA) (funding number ZT-I-OO1 4) and supported by NSFC under Grant 62132011.

REFERENCES

[1] https://www.cs.toronto.edu/~kriz/cifar.html.

[2] Mohamed S Abdelfattah, Abhinav Mehrotra, Łukasz Dudziak, and Nicholas Donald Lane. Zero-Cost Proxies for Lightweight {NAS}. In *International Conference on Learning Representations (ICLR)*, 2021.

[3] Bowen Baker, Otkrist Gupta, Nikhil Naik, and Ramesh Raskar. Designing Neural Network Architectures using Reinforcement Learning. In *International Conference on Learning Representations (ICLR)*, 2017.

[4] Tom B. Brown, Benjamin Mann, Nick Ryder, Melanie Subbiah, Jared Kaplan, Prafulla Dhariwal, Arvind Neelakantan, Pranav Shyam, Girish Sastry, Amanda Askell, Sandhini Agarwal, Ariel Herbert-Voss, Gretchen Krueger, Tom Henighan, Rewon Child, Aditya Ramesh, Daniel M. Ziegler, Jeffrey Wu, Clemens Winter, Christopher Hesse, Mark Chen, Eric Sigler, Mateusz Litwin, Scott Gray, Benjamin Chess, Jack Clark, Christopher Berner, Sam McCandlish, Alec Radford, Ilya Sutskever, and Dario Amodei. Language Models are Few-Shot Learners. In *Annual Conference on Neural Information Processing Systems (NeurIPS)*. NeurIPS, 2020.

[5] Han Cai, Jiacheng Yang, Weinan Zhang, Song Han, and Yong Yu. Path-Level Network Transformation for Efficient Architecture Search. In *International Conference on Machine Learning (ICML)*. PMLR, 2018.

[6] Dingfan Chen, Ning Yu, Yang Zhang, and Mario Fritz. GAN-Leaks: A Taxonomy of Membership Inference Attacks against Generative Models. In *ACM SIGSAC Conference on Computer and Communications Security (CCS)*, pages 343–362. ACM, 2020.

[7] Min Chen, Zhikun Zhang, Tianhao Wang, Michael Backes, Mathias Humbert, and Yang Zhang. When Machine Unlearning Jeopardizes Privacy. In *ACM SIGSAC Conference on Computer and Communications Security (CCS)*, pages 896–911. ACM, 2021.

[8] Min Chen, Zhikun Zhang, Tianhao Wang, Michael Backes, Mathias Humbert, and Yang Zhang. Graph Unlearning. In *ACM SIGSAC Conference on Computer and Communications Security (CCS)*. ACM, 2022.

[9] Tianqi Chen and Carlos Guestrin. XGBoost: A Scalable Tree Boosting System. In *ACM Conference on Knowledge Discovery and Data Mining (KDD)*, pages 785–794. ACM, 2016.

[10] Wuyang Chen, Xinyu Gong, and Zhangyang Wang. Neural Architecture Search on ImageNet in Four {GPU} Hours: A Theoretically Inspired Perspective. In *International Conference on Learning Representations (ICLR)*, 2021.

[11] Xiangning Chen and Cho-Jui Hsieh. Stabilizing Differentiable Architecture Search via Perturbation-based Regularization. In *International Conference on Machine Learning (ICML)*. PMLR, 2020.

[12] Xiangning Chen, Ruochen Wang, Minhao Cheng, Xiaocheng Tang, and Cho-Jui Hsieh. DrNAS: Dirichlet Neural Architecture Search. In *International Conference on Learning Representations (ICLR)*, 2021.

[13] Christopher A. Choquette Choo, Florian Tramèr, Nicholas Carlini, and Nicolas Papernot. Label-Only Membership Inference Attacks. In *International Conference on Machine Learning (ICML)*, pages 1964–1974. PMLR, 2021.

[14] Adam Coates, Andrew Y. Ng, and Honglak Lee. An Analysis of Single-Layer Networks in Unsupervised Feature Learning. In *International Conference on Artificial Intelligence and Statistics (AISTATS)*, pages 215–223. JMLR, 2011.

[15] Chaitanya Devaguptapu, Devansh Agarwal, Gaurav Mittal, Pulkit Gopalani, and Vineeth N Balasubramanian. On Adversarial Robustness: A Neural Architecture Search Perspective. In *IEEE International Conference on Computer Vision Workshops (ICCVW)*, pages 152–161. IEEE/CVF, 2021.

[16] Xuanyi Dong and Yi Yang. One-Shot Neural Architecture Search via Self-Evaluated Template Network. In *IEEE International Conference on Computer Vision (ICCV)*, pages 3681–3690. IEEE, 2019.

[17] Xuanyi Dong and Yi Yang. Searching for A Robust Neural Architecture in Four GPU Hours. In *IEEE Conference on Computer Vision and Pattern Recognition (CVPR)*, pages 1761–1770. IEEE, 2019.

[18] Xuanyi Dong and Yi Yang. NAS-Bench-201: Extending the Scope of Reproducible Neural Architecture Search. In *International Conference on Learning Representations (ICLR)*, 2020.

[19] Harris Drucker, Chris J.C. Burges, Linda Kaufman, Alex Smola, and Vladimir Vapnik. Support Vector Regression Machines. In *Annual Conference on Neural Information Processing Systems (NIPS)*, page 155–161. NIPS, 1996.

[20] Linkang Du, Zhikun Zhang, Shaojie Bai, Changchang Liu, Shouling Ji, Peng Cheng, and Jiming Chen. AHEAD: Adaptive Hierarchical Decomposition for Range Query under Local Differential Privacy. In *ACM SIGSAC Conference on Computer and Communications Security (CCS)*, page 1266–1288. ACM, 2021.

[21] Cynthia Dwork, Frank McSherry, Kobbi Nissim, and Adam Smith. Calibrating Noise to Sensitivity in Private Data Analysis. In *Theory of Cryptography Conference (TCC)*, pages 265–284. Springer, 2006.

[22] Golnaz Ghiasi, Tsung-Yi Lin, and Quoc V. Le. NAS-FPN: Learning Scalable Feature Pyramid Architecture for Object Detection. In *IEEE Conference on Computer Vision and Pattern Recognition (CVPR)*, pages 7036–7045. IEEE, 2019.

[23] Yu-Chao Gu, Li-Juan Wang, Yun Liu, Yi Yang, Yu-Huan Wu, Shao-Ping Lu, and Ming-Ming Cheng. DOTS: Decoupling Operation and Topology in Differentiable Architecture Search. In *IEEE Conference on Computer Vision and Pattern Recognition (CVPR)*. IEEE, 2021.

[24] Minghao Guo, Yuzhe Yang, Rui Xu, Ziwei Liu, and Dahua Lin. When NAS Meets Robustness: In Search of Robust Architectures against Adversarial Attacks. In *IEEE Conference on Computer Vision and Pattern Recognition (CVPR)*, pages 631–640. IEEE, 2020.

[25] Kaiming He, Xiangyu Zhang, Shaoqing Ren, and Jian Sun. Deep Residual Learning for Image Recognition. In *IEEE Conference on Computer Vision and Pattern Recognition (CVPR)*, pages 770–778. IEEE, 2016.

[26] Xinlei He, Rui Wen, Yixin Wu, Michael Backes, Yun Shen, and Yang Zhang. Node-Level Membership Inference Attacks Against Graph Neural Networks. *CoRR abs/2102.05429*, 2021.

[27] Tin Kam Ho. Random decision forests. In *Proceedings of the 3rd International Conference on Document Analysis and Recognition*, volume 1, pages 278–282. IEEE, 1995.

[28] Andrew G. Howard, Menglong Zhu, Bo Chen, Dmitry Kalenichenko, Weijun Wang, Tobias Weyand, Marco Andreetto, and Hartwig Adam. MobileNets: Efficient Convolutional Neural Networks for Mobile Vision Applications. *CoRR abs/1704.04681*, 2017.

[29] Hongsheng Hu, Zoran Salcic, Lichao Sun, Gillian Dobbie, Philip S. Yu, and Xuyun Zhang. Membership Inference Attacks on Machine Learning: A Survey. *ACM Computing Surveys*, 2021.

[30] Gao Huang, Zhuang Liu, Laurens van der Maaten, and Kilian Q. Weinberger. Densely Connected Convolutional Networks. In *IEEE Conference on Computer Vision and Pattern Recognition (CVPR)*, pages 2261–2269. IEEE, 2017.

[31] Hai Huang, Zhikun Zhang, Yun Shen, Michael Backes, Qi Li, and Yang Zhang. On the Privacy Risks of Cell-Based NAS Architectures. *CoRR abs/2209.01688*, 2022.

[32] Bargav Jayaraman and David Evans. Evaluating Differentially Private Machine Learning in Practice. In *USENIX Security Symposium (USENIX Security)*, pages 1895–1912. USENIX, 2019.

[33] Jinyuan Jia, Ahmed Salem, Michael Backes, Yang Zhang, and Neil Zhenqiang Gong. MemGuard: Defending against Black-Box Membership Inference Attacks via Adversarial Examples. In *ACM SIGSAC Conference on Computer and Communications Security (CCS)*, pages 259–274. ACM, 2019.

[34] Yigitcan Kaya and Tudor Dumitras. When Does Data Augmentation Help With Membership Inference Attacks? In *International Conference on Machine Learning (ICML)*, pages 5345–5355. PMLR, 2021.

[35] Guolin Ke, Qi Meng, Thomas Finley, Taifeng Wang, Wei Chen, Weidong Ma, Qiwei Ye, and Tie-Yan Liu. LightGBM: A Highly Efficient Gradient Boosting Decision Tree. In *Annual Conference on Neural Information Processing Systems (NIPS)*. NIPS, 2017.

[36] Yoon Kim. Convolutional Neural Networks for Sentence Classification. In *Conference on Empirical Methods in Natural Language Processing (EMNLP)*, page 1746–1751. ACL, 2014.

[37] Alexander Kolesnikov, Lucas Beyer, Xiaohua Zhai, Joan Puigcerver, Jessica Yung, Sylvain Gelly, and Neil Houlsby. Big Transfer (BiT): General Visual Representation Learning. In *European Conference on Computer Vision (ECCV)*, pages 491–507. Springer, 2020.

[38] Alex Krizhevsky, Ilya Sutskever, and Geoffrey E. Hinton. ImageNet Classification with Deep Convolutional Neural Networks. In *Annual Conference on Neural Information Processing Systems (NIPS)*, pages 1106–1114. NIPS, 2012.

[39] Hayeon Lee, Eunyoung Hyung, and Sung Ju Hwang. Rapid Neural Architecture Search by Learning to Generate Graphs from Datasets. In *International Conference on Learning Representations (ICLR)*, 2021.

[40] Hao Li, Zheng Xu, Gavin Taylor, Christoph Studer, and Tom Goldstein. Visualizing the Loss Landscape of Neural Nets. In *Annual Conference on Neural Information Processing Systems (NeurIPS)*. NeurIPS, 2018.

[41] Yanxi Li, Zhaohui Yang, Yunhe Wang, and Chang Xu. Neural Architecture Dilation for Adversarial Robustness. In *Annual Conference on Neural Information Processing Systems (NeurIPS)*. NeurIPS, 2021.

[42] Zheng Li, Yiyong Liu, Xinlei He, Ning Yu, Michael Backes, and Yang Zhang. Auditing Membership Leakages of Multi-Exit Networks. *CoRR abs/2208.11180*, 2022.

[43] Zheng Li and Yang Zhang. Membership Leakage in Label-Only Exposures. In *ACM SIGSAC Conference on Computer and Communications Security (CCS)*, pages 880–895. ACM, 2021.

[44] Hanxiao Liu, Karen Simonyan, and Yiming Yang. DARTS: Differentiable Architecture Search. In *International Conference on Learning Representations (ICLR)*, 2019.

[45] Hongbin Liu, Jinyuan Jia, Wenjie Qu, and Neil Zhenqiang Gong. EncoderMI: Membership Inference against Pre-trained Encoders in Contrastive Learning. In *ACM SIGSAC Conference on Computer and Communications Security (CCS)*. ACM, 2021.

[46] Wei Liu, Dragomir Anguelov, Dumitru Erhan, Christian Szegedy, Scott Reed, Cheng-Yang Fu, and Alexander C. Berg. SSD: Single Shot MultiBox Detector. In *European Conference on Computer Vision (ECCV)*, pages 21–37. Springer, 2016.

[47] Yugeng Liu, Rui Wen, Xinlei He, Ahmed Salem, Zhikun Zhang, Michael Backes, Emiliano De Cristofaro, Mario Fritz, and Yang Zhang. ML-Doctor: Holistic Risk

Assessment of Inference Attacks Against Machine Learning Models. In *USENIX Security Symposium (USENIX Security)*. USENIX, 2022.
[48] Ziwei Liu, Ping Luo, Xiaogang Wang, and Xiaoou Tang. Deep Learning Face Attributes in the Wild. In *IEEE International Conference on Computer Vision (ICCV)*, pages 3730–3738. IEEE, 2015.
[49] Andreas Loukas. What Graph Neural Networks Cannot Learn: Depth vs Width. In *International Conference on Learning Representations (ICLR)*, 2020.
[50] Zhou Lu, Hongming Pu, Feicheng Wang, Zhiqiang Hu, and Liwei Wang. The Expressive Power of Neural Networks: A View from the Width. In *Annual Conference on Neural Information Processing Systems (NIPS)*. NIPS, 2017.
[51] Milad Nasr, Reza Shokri, and Amir Houmansadr. Machine Learning with Membership Privacy using Adversarial Regularization. In *ACM SIGSAC Conference on Computer and Communications Security (CCS)*, pages 634–646. ACM, 2018.
[52] Milad Nasr, Reza Shokri, and Amir Houmansadr. Comprehensive Privacy Analysis of Deep Learning: Passive and Active White-box Inference Attacks against Centralized and Federated Learning. In *IEEE Symposium on Security and Privacy (S&P)*, pages 1021–1035. IEEE, 2019.
[53] Samet Oymak, Mingchen Li, and Mahdi Soltanolkotabi. Generalization Guarantees for Neural Architecture Search with Train-Validation Split. In *International Conference on Machine Learning (ICML)*, pages 8291–8301. PMLR, 2021.
[54] Ren Pang, Zhaohan Xi, Shouling Ji, Xiapu Luo, and Ting Wang. On the Security Risks of AutoML. In *USENIX Security Symposium (USENIX Security)*. USENIX, 2022.
[55] Hieu Pham, Melody Y. Guan, Barret Zoph, Quoc V. Le, and Jeff Dean. Efficient Neural Architecture Search via Parameter Sharing. In *International Conference on Machine Learning (ICML)*. PMLR, 2018.
[56] Alec Radford, Karthik Narasimhan, Tim Salimans, and Ilya Sutskever. Improving language understanding by generative pre-training. 2018.
[57] Alec Radford, Jeffrey Wu, Rewon Child, David Luan, Dario Amodei, and Ilya Sutskever. Language Models are Unsupervised Multitask Learners. *OpenAI blog*, 2019.
[58] Ilija Radosavovic, Raj Prateek Kosaraju, Ross Girshick, Kaiming He, and Piotr Dollár. Designing Network Design Spaces. In *IEEE Conference on Computer Vision and Pattern Recognition (CVPR)*, pages 10428–10436. IEEE, 2020.
[59] Aditya Ramesh, Mikhail Pavlov, Gabriel Goh, Scott Gray, Chelsea Voss, Alec Radford, Mark Chen, and Ilya Sutskever. Zero-Shot Text-to-Image Generation. In *International Conference on Machine Learning (ICML)*, pages 8821–8831. JMLR, 2021.
[60] Shaoqing Ren, Kaiming He, Ross Girshick, and Jian Sun. Faster R-CNN: Towards Real-Time Object Detection with Region Proposal Networks. *CoRR abs/1506.01497*, 2015.
[61] Itay Safran and Ohad Shamir. Depth-Width Tradeoffs in Approximating Natural Functions with Neural Networks. In *International Conference on Machine Learning (ICML)*, pages 2979–2987. PMLR, 2017.
[62] Ahmed Salem, Yang Zhang, Mathias Humbert, Pascal Berrang, Mario Fritz, and Michael Backes. ML-Leaks: Model and Data Independent Membership Inference Attacks and Defenses on Machine Learning Models. In *Network and Distributed System Security Symposium (NDSS)*. Internet Society, 2019.
[63] Virat Shejwalkar and Amir Houmansadr. Membership Privacy for Machine Learning Models Through Knowledge Transfer. In *AAAI Conference on Artificial Intelligence (AAAI)*, pages 9549–9557. AAAI, 2021.
[64] Reza Shokri, Marco Stronati, Congzheng Song, and Vitaly Shmatikov. Membership Inference Attacks Against Machine Learning Models. In *IEEE Symposium on Security and Privacy (S&P)*, pages 3–18. IEEE, 2017.
[65] Yao Shu, Wei Wang, and Shaofeng Cai. Understanding Architectures Learnt by Cell-based Neural Architecture Search. In *International Conference on Learning Representations (ICLR)*, 2020.
[66] Julien Siems, Lucas Zimmer, Arber Zela, Jovita Lukasik, Margret Keuper, and Frank Hutter. NAS-Bench-301 and the Case for Surrogate Benchmarks for Neural Architecture Search. *CoRR abs/2008.09777*, 2020.
[67] Karen Simonyan and Andrew Zisserman. Very Deep Convolutional Networks for Large-Scale Image Recognition. In *International Conference on Learning Representations (ICLR)*, 2015.
[68] Christian Szegedy, Vincent Vanhoucke, Sergey Ioffe, Jonathon Shlens, and Zbigniew Wojna. Rethinking the Inception Architecture for Computer Vision. In *IEEE Conference on Computer Vision and Pattern Recognition (CVPR)*, pages 2818–2826. IEEE, 2016.
[69] Mingxing Tan and Quoc V. Le. EfficientNet: Rethinking Model Scaling for Convolutional Neural Networks. In *International Conference on Machine Learning (ICML)*. PMLR, 2019.
[70] Xingchen Wan, Binxin Ru, Pedro M Esperança, and Zhenguo Li. On Redundancy and Diversity in Cell-based Neural Architecture Search. In *International Conference on Learning Representations (ICLR)*, 2022.
[71] Chien-Yao Wang, Hong-Yuan Mark Liao, I-Hau Yeh, Yueh-Hua Wu, Ping-Yang Chen, and Jun-Wei Hsieh. CSPNet: A New Backbone that can Enhance Learning Capability of CNN. In *IEEE Conference on Computer Vision and Pattern Recognition Workshops (CVPRW)*, pages 1571–1580. IEEE, 2020.
[72] Ning Wang, Yang Gao, Hao Chen, Peng Wang, Zhi Tian, Chunhua Shen, and Yanning Zhang. NAS-FCOS: Fast Neural Architecture Search for Object Detection. In *IEEE Conference on Computer Vision and Pattern Recognition (CVPR)*, pages 11943–11951. IEEE, 2020.
[73] Ruochen Wang, Minhao Cheng, Xiangning Chen, Xiaocheng Tang, and Cho-Jui Hsieh. Rethinking Architecture Selection in Differentiable NAS. In *International Conference on Learning Representations (ICLR)*, 2021.
[74] Tianhao Wang, Joann Qiongna Chen, Zhikun Zhang, Dong Su, Yueqiang Cheng, Zhou Li, Ninghui Li, and Somesh Jha. Continuous Release of Data Streams under both Centralized and Local Differential Privacy. In *ACM SIGSAC Conference on Computer and Communications Security (CCS)*, page 1237–1253. ACM, 2021.
[75] Colin White, Willie Neiswanger, and Yash Savani. BANANAS: Bayesian Optimization with Neural Architectures for Neural Architecture Search. In *AAAI Conference on Artificial Intelligence (AAAI)*, pages 10293–10301. AAAI, 2021.
[76] Saining Xie, Ross Girshick, Piotr Dollár, Zhuowen Tu, and Kaiming He. ResNeXt: Aggregated Residual Transformations for Deep Neural Networks. In *IEEE Conference on Computer Vision and Pattern Recognition (CVPR)*. IEEE, 2017.
[77] Keyulu Xu, Weihua Hu, Jure Leskovec, and Stefanie Jegelka. How Powerful are Graph Neural Networks? In *International Conference on Learning Representations (ICLR)*, 2019.
[78] Yuhui Xu, Lingxi Xie, Xiaopeng Zhang, Xin Chen, Guo-Jun Qi, Qi Tian, and Hongkai Xiong. Partial Channel Connections for Memory-Efficient Differentiable Architecture Search. In *International Conference on Learning Representations (ICLR)*, 2020.
[79] Liang Yao, Chengsheng Mao, and Yuan Luo. Graph Convolutional Networks for Text Classification. In *AAAI Conference on Artificial Intelligence (AAAI)*, page 7370–7377. AAAI, 2019.
[80] Samuel Yeom, Irene Giacomelli, Matt Fredrikson, and Somesh Jha. Privacy Risk in Machine Learning: Analyzing the Connection to Overfitting. In *IEEE Computer Security Foundations Symposium (CSF)*, pages 268–282. IEEE, 2018.
[81] Fisher Yu, Dequan Wang, Evan Shelhamer, and Trevor Darrell. Deep Layer Aggregation. In *IEEE Conference on Computer Vision and Pattern Recognition (CVPR)*, pages 2403–2412. IEEE, 2018.
[82] Sergey Zagoruyko and Nikos Komodakis. Wide Residual Networks. In *Proceedings of the British Machine Vision Conference (BMVC)*. BMVA Press, 2016.
[83] Minxing Zhang, Zhaochun Ren, Zihan Wang, Pengjie Ren, Zhumin Chen, Pengfei Hu, and Yang Zhang. Membership Inference Attacks Against Recommender Systems. In *ACM SIGSAC Conference on Computer and Communications Security (CCS)*, pages 864–879. ACM, 2021.
[84] Zhikun Zhang, Tianhao Wang, Jean Honorio, Ninghui Li, Michael Backes, Shibo He, Jiming Chen, and Yang Zhang. PrivSyn: Differentially Private Data Synthesis. In *USENIX Security Symposium (USENIX Security)*, pages 929–946. USENIX, 2021.
[85] Zhikun Zhang, Tianhao Wang, Ninghui Li, Shibo He, and Jiming Chen. CALM: Consistent Adaptive Local Marginal for Marginal Release under Local Differential Privacy. In *ACM SIGSAC Conference on Computer and Communications Security (CCS)*, page 212–229. ACM, 2018.
[86] Barret Zoph and Quoc V. Le. Neural Architecture Search with Reinforcement Learning. *CoRR abs/1611.01578*, 2016.
[87] Barret Zoph, Vijay Vasudevan, Jonathon Shlens, and Quoc V. Le. Learning Transferable Architectures for Scalable Image Recognition. In *IEEE Conference on Computer Vision and Pattern Recognition (CVPR)*, pages 8697–8710. IEEE, 2018.